Incorporating the logistic regression into a decision-centric framework for probabilistic assessment of climate change impacts on a complex water system

Daeha Kim[1], Jong Ahn Chun[1], Si-Jung Choi[2]

[1]APEC Climate Center, Busan, 48058, South Korea
[2]Korea Institute of Civil Engineering and Building Technology, Gyeonggi-do, 10223, South Korea

Correspondence to: Si-Jung Choi (sjchoi@kict.re.kr)

Abstract. Climate change is a global stressor that can undermine water management policies developed with the assumption of stationary climate. While the response-surface-based assessments provided a new paradigm for formulating actionable adaptive solutions, the uncertainty associated with the stress tests pose challenges. To address the risks of unsatisfactory performances in a domain of climate stresses, this study proposed to incorporate the logistic regression into a decision-centric framework. The proposed approach replaces the "responses surfaces" of the performance metrics typically used for the decision scaling framework with the "logistic surfaces" that describes the risk of system failures against pre-defined performance thresholds. As a case study, water supply and environmental reliabilities were assessed within the eco-engineering decision scaling framework for a complex river basin in South Korea. Results showed that human-demand-only operations in the river basin could result in water deficiency at a location requiring ecological flows. To reduce the environmental risks, the stakeholders should accept increasing risks of unsatisfactory water supply perforamnce at the sub-basins with small water demands. This study suggests that the logistic surfaces could provide convenience to measure system robustness to climatic changes from multiple perspectives together with the risk information for decision-making processes.

1 Introduction

Climate change is a global stressor that poses prodigious challenges to long-term management of water resources. While water infrastructures have been constructed across the globe to sustain human livelihood and activities, those assets have been traditionally managed by heuristic operation policies developed under the assumption of stationary climate (Cosgrove and Loucks, 2015; Cully et al., 2016). However, probabilistic behaviours of hydrological processes can be significantly altered by the warming atmosphere; thereby, the heuristic management is expected to become increasingly vulnerable (Brown et al., 2015; Georgakakos et al., 2012).

When formulating management solutions to non-stationary climate for a water system, an essential step is to assess impacts of climate change on its performance. An established method for the impact assessment was to investigate outputs of relevant system models forced by projections of the general circulation models (GCMs) under hypothetical greenhouse gas

(GHG) emission scenarios (e.g., Xu et al., 2015; Eum and Simonovic, 2010). This type of assessments takes the 'predict-then-act' paradigm for which the first prerequisite is sufficiently reliable predictions. The GCM projections, however, are often biased by inappropriate model formulations and/or imperfectly understood physical processes (Stevens and Bony, 2013; Deser et al., 2012; Dufresne and Bony, 2008; Stainforth et al., 2005). Thus, they may contain unacceptably high risk costs for policymakers (Brown et al. 2012), leading to underutilization of GCM-led strategies (Weaver et al., 2013; Brown and Wilby, 2012).

To overcome the weakness of GCM-driven assessments in practical decision support, alternative frameworks within the 'robust decision' paradigm have emerged (e.g., Hadka et al., 2015; Whateley et al., 2014; Lampert and Groves, 2010). These decision-centric approaches seek robust solutions that can minimize adverse effects of climatic stresses on given hydrological systems. Examples include the decision scaling (Brown et al., 2012), the dynamic adaptive policy pathways (Haasnoot et al., 2013), the real option analysis (Woodward et al., 2014), the Info-gap decision theory (Korteling et al., 2013), and the robust decision making (Lempert and Groves, 2010) among others. Whereas the 'predict-then-act' paradigm focus on the most likely future conditions that can maximize expected utility, the decision-centric approaches pay attention to sensitivity (or vulnerability) of system performance to climatic stressors (Weaver et al., 2013; Brown et al., 2012). This paradigm accepts the irreducible uncertainty in climate predictions as an inevitable part of long-term planning, and guide decision-makers toward low-regret strategies for sustainable system performance under non-stationary climate.

Among the decision-centric frameworks, the assessments based on the response functions of system performance have provided convenience to define decision thresholds at which adaptation actions are required (e.g., Kim et al., 2018; Steinschneider et al., 2015a; Turner et al., 2014; Whateley et al., 2014; Brown et al., 2012; Prudhomme et al., 2010). They developed the relationships between system performances and climatic stressors (hereafter referred to as the "response surfaces") via stress tests. Then, GCM projections were employed to indicate future system performance on the response surfaces. The response-surface-based methods have been refined to consider spatially varying system performance (e.g., Schlef et al., 2018) and multiple management objectives within a hydrological system (e.g., Cully et al., 2016). They allowed efficient evaluation of climate change risks simply by comparing the performance metrics indicated by a collection of GCMs against pre-defined thresholds.

Nonetheless, uncertainty of the response surfaces cannot be neglected due to assumptions and simplifications associated with the stress tests (Kay et al., 2014). Indeed, Steinschneider et al. (2015b) argued that hydrological modelling and climatic variability may introduce uncertainty in the response surfaces as much as GCM projections. Kim et al. (2018) showed how climate change risks can be underestimated when a modelling scale was inappropriately chosen. Hence, over-reliance on the response surfaces of general performance metrics may misguide users to inappropriate and/or untimely adaptation policies. Importantly, the response surfaces have usually been developed with climatic shifts defined by long-term changes in statistical moments of weather observations (e.g.,Poff et al., 2016; Steinschneider et al., 2015a; Whateley et al., 2014; Turner et al., 2014), even though they might insufficiently explain variation of chosen performance indicators.

Whateley and Brown (2016) found that water supply system performance can be attributed mostly to uncertainty in internal climate variability over a time horizon of policy planning.

The prior studies imply that risks of system failures still exists even in the climate zone of satisfactory performance in the response surfaces. This uncertainty issue may be mended in part by evaluating the risks of system failures along with the response surfaces of expected performances. While it is possible to conduct stochastic uncertainty analyses with the stress tests (e.g., Steinschneider et al., 2015b; Whateley and Brown, 2016), this approach would require expensive computational costs even with modern computing power (Whateley et al., 2016). In this work, therefore, an efficient approach was proposed to evaluate the risks of system failures within a decision-centric framework. We simply incorporated the logistic regression into typical stress tests for the response-surface-based assessments. As a case study, here we provided a slightly modified version of the eco-engineering decision scaling framework (Poff et al., 2016) to explore the probabilities of system failures varying across a complex river system with two contrasting management purposes.

2 Methodology

2.1 Eco-engineering decision scaling framework

The eco-engineering decision scaling (EEDS) framework (Poff et al., 2016) expanded the decision scaling (Brown et al., 2012) to consider stakeholders' multifaceted interests in the response surfaces. Iterative five-steps are required for this framework. Step 1 is to identify possible management options (e.g., upgrading operations and/or structural investments), to select indicators of ecological and engineering performances (e.g., water supply reliability and ecological vulnerability), and to define user-specific thresholds under which the system performs unacceptably. Step 2 is to build system models for the hypothetical stress tests. For water resources management, the system models may include a runoff model and a water allocation model. By exposing the system models to a wide range of hypothetical climatic stressors (x_i), ecological and engineering performances can be evaluated. In step 3, the response surfaces of engineering and ecological performances are developed with outcomes of the stress tests. For vulnerability analysis, the pre-defined thresholds are imposed on the response surfaces. Step 4 is to evaluate the management options with the size of the climatic zones satisfying the performance thresholds. In step 5, preferred decisions for the management options can be made. Or, if necessary, the assessment from step 1 to 4 can be repeated with new management options and/or different criteria.

In the EEDC framework, the key information would be the size of the climate zone mutually satisfying the engineering and ecological thresholds since it measures overall system robustness to climate stresses. Decision-makers may prefer management options that can widen the mutual climate zone, if they are socio-economically viable. However, the system robustness is not the only criterion for selecting management options. In decision-making processes, questions can be raised such as "what if future climates will not fall within the mutual climate zone?" and "how much risks of system failures still exist within the climate zone that expects satisfactory performances?" Those questions can be answered by incorporating the logistic regression and a collection of GCM projections into the EEDC framework.

2.2 Incorporating the logistic regression into the stress tests

The stress tests in step 3 for the EEDC framework are intended to find expected performances per given climate exposure. By comparing the obtained performances against a pre-defined threshold, the climate exposures applied to the stress tests can be categorized into binary outcomes (i.e., 1 for satisfactory performances and 0 for otherwise). With no needs of the homogeneity and normality assumptions, the logistic regression model allows to explain occurrences of the satisfactory performances with the sigmoid function of the climate exposures (x_i):

$$\pi = \frac{1}{1+\exp[-(\beta_0+\beta_1 x_1+\beta_2 x_2+\cdots)]} \quad (1)$$

where, π is the probability of satisfactory performance, and β_i are the regression coefficients. Thus, 1-π becomes the probability of unsatisfactory performance.

When two explanatory variables are chosen for x_i (e.g., changes in mean annual precipitation and temperature), it is possible to develop a 2-dimensional surface to describe variation of π within a climate domain. Hereafter, the surface of π will be referred to as the "logistic surface". In this study, the logistic surfaces were used for the steps 3 and 4 of the EEDC framework in lieu of the response surfaces. The following example shows how to assess the risk of system failures together with robustness to climate stresses for a complex water system.

3 Application: A case study for optimal water allocation in a complex water system

3.1 Study area

The case study area is the Geum River Basin located in the west-central part of South Korea with a total area of 9,915 km^2 (Figure 1). The mean and the highest elevations in the river basin are 85 m and 1,596 m above the sea level, respectively. The mean basin slope is 16.7%. The total length of the main channel is approximately 402 km. The river basin has a semi-humid climate with monsoonal summer seasons. Wet air masses moving from the North Pacific usually make hot and humid summer seasons, whereas winter seasons are dry and cold due to the Siberian high pressure. Approximately, 60-70% of annual precipitation falls in June to September (KMA, 2011); thus, river flows across the basin peaks in the middle of summer monsoon seasons. Snowmelt runoff minimally contributes to streamflow variations due to small winter precipitation (Bae et al., 2008).

The Geum River Basin is officially divided into 14 sub-basins for administrative purposes along the geomorphological boundaries. The sub-basin areas vary between 120 and 1,856 km^2 with an average of 708 km^2. 60% of the entire river basin is covered by forests, while agricultural areas account for 18%. The forest covers and agricultural lands within the 14 sub-basins occupy 33-83% and 4.6-42%, respectively. The sub-basins with relatively large agricultural lands tend to have small forest covers. The urban areas are 5.3% of the river basin in total. According to the Korea Forest Service (http://forest.go.kr),

the soils across the Geum River Basin have moderate to high infiltration capacity, implying sub-surface runoff generations are dominant.

Human interventions affect the flow regimes in the Geum River Basin. The main channel is regulated by two large dams serially connected for water supplies and flood controls. The Yongdam Dam located in the upper river basin has an effective storage capacity of 809 Mm^3, while the Daecheong Dam at the middle of the main channel has a larger capacity of 1,040 Mm^3. Water storages in both dams are delivered to several sub-basins through water distribution systems developed for municipal and industrial (M&I) water demands, making non-geomorphological human-made connectivity between the sub-basins. The two large dams supply water to the demand sectors in outsides of the river basin through the distribution systems; hence, inter-basin water transfers may conflict with water demands within the river basin. During monsoon seasons, Yongdam and Dacheong Dams should reduce their storage limits by 137 Mm^3 and 250 Mm^3 for flood control, respectively. In addition, many small-size local reservoirs are widespread across the river basin to sustain irrigated agriculture (mostly for planting paddy rice). Though 95% of the small reservoirs have minimal storage capacities below 1 Mm^3, their gross capacity is more than 320 Mm^3 and thus considerably alters natural flow regimes. The total storage capacities of the agricultural reservoirs in the 14 sub-basins are from 1.1 Mm^3 to 100.9 Mm^3 with a median value of 12.5 Mm^3. In each sub-basin, natural river flows and water transferred from the storage facilities (i.e., the agricultural reservoirs and dams) are consumed for agricultural, and municipal and industrial purposes. The water diverted for the M&I demands could return to the rivers, becoming available water for lower demand sectors.

For water allocation modelling, we simplified the complex river system with a node-and-link network shown in Figure 1. Each sub-basin was conceptualized as a node with natural water availability (i.e., natural runoff), storage capacity (i.e., water storage in the agricultural reservoirs), and water demands (i.e., agricultural and M&I water uses). The sub-basin nodes were connected by the stream links (the continuous lines). The two large dams were represented by the nodes only having storage capacities and located between the two adjacent sub-basins accordingly. The outside water demands sectors were represented by nodes with no natural flows and zero storage capacities. The human-made connections between the dams and the sub-basins were conceptualized by separate links (the dashed lines) with conveyance limits.

3.2 Data collections

3.2.1 Climate and water demand data

We collected daily precipitation and maximum and minimum temperatures over South Korea at 3-km grid resolution for 1973-2015. The grid data were produced by interpolating synoptic observations at 60 stations in the automated surface observing system (ASOS) operated by the Korea Meteorological Administration. The point weather data were spatially interpolated by the Parameter-elevation Regression on Independent Slope Model (PRISM; Daly et al., 2008), and overestimated values were smoothed by the inverse distance method. Jung and Eum (2015) found improved performance of the combined method in South Korea via comparative evaluations to the original PRISM. For the case study, the collected

grid data were spatially aggregated with the sub-basin boundaries. The aggregated daily precipitation and temperature were perturbed by a stochastic weather generator for the stress tests, and then used to generate streamflow at the sub-basin nodes. According to the grid data, the mean annual precipitation and temperature over the Geum River Basin for 1976-1995 were 1,245 mm and 11.7 ℃, respectively. They have risen to 1,325 mm (+6.4%) and 12.2 ℃ (+0.5℃) during 1996-2015, providing an indication that atmospheric water supply and demand gradually increase over time within the river basin.

The water demands for 2030 were taken as the reference demands to evaluate water allocation performance across the river basin. In South Korea, government-driven national water resources plans are legally developed for sustainable resources management for every bi-decadal period. The water resources plan for 2020 was first established in 2000 including water demand projections up to 2020 (MOCT, 2000), and has been revised three times to consider hydrologic and socioeconomic changes since the initial version (MOCT, 2006; MLTM, 2011; MOLIT, 2016). In the third version of the water resources plan for 2020 (MOLIT, 2016), the water demands across South Korea were re-projected up to 2030. By electronic correspondence (requested on Sep-26/2017), we obtained the demand data projected to 2030 given at 10-day intervals for the sub-basins and the two outside nodes directly linked to sub-basins from the team leading the national water plan at the Korea Institute of Civil Engineering and Building Technology. Among the high, standard, low demand scenarios given in MOLIT (2016), we chose the high demand scenario from a conservative perspective. More details about the demand projections are available in MOLIT (2016**)**. The M&I demands at the two outside nodes connected with the two dams were estimated by the water transfer records for simplicity.

In addition, we collected the information of the minimum flow rates required for ecosystem sustainability, namely "instreamflows" (Jowett, 1997), at seven locations within the river basin. The instreamflows are determined by the experts' investigations into water quality and ecological conditions in the vicinity of major rivers in South Korea, and officially announced by the Ministry of Environment and the Ministry of Land, Infrastructure, and Transport (MOLIT, 2016). Though the human water demands (i.e., agricultural and M&I uses) are the first priority of the local and regional authorities (MOLIT, 2016), they are recommended to consider the instreamflows for environmental sustainability. Table 1 summarizes the agricultural and M&I demands for the year of 2030 and the instreamflow requirements. For water allocation modelling, the demand data at 10-day interval were aggregated into monthly values.

3.2.2 Bias-corrected GCM projections

Daily precipitation and temperature projections of 25 GCMs (Table A1) were collected from the archive of the Coupled Model Intercomparison Project Phase 5 (Taylor et al., 2012). Two representative concentration pathways (RCPs), RCP4.5 and RCP8.5, were selected to assess the water supply capacity of the river basin for the upcoming bi-decadal period of 2020-2039. RCP4.5 and RCP8.5 were used as scenarios of stabilized and increasing greenhouse gas concentrations frequently in climate change studies (e.g., Yan et al., 2015; Zhang et al., 2016; Moursi et al., 2017).

The 50 GCM projections (i.e., 25 GCMs×2 RCPs) were bias-corrected by the de-trended quantile mapping (DQM; Bürger et al., 2013; Eum and Cannon, 2017) that can preserve raw climate change signals given by GCMs. The DQM removes the

long-term mean change in projected values first. After applying the ordinary quantile mapping (QM; e.g., Hwang and Graham, 2013) to the de-trended values, the removed trend is reintroduced to the bias-corrected projections. The de-trending procedure may prevent the exaggeration of raw climate change signals, which is a typical drawback of the ordinary QM. More details about DQM and related bias correction methods are available in Bürger et al. (2013), Cannon et al. (2015), and Eum and Cannon (2017). To correct the 50 GCM projections toward the spatial averaged precipitation and temperatures over the Geum River Basin, 1976-2005 and 2006-2099 were set as the reference and the projection periods, respectively.

3.3 Stress tests for water allocation performances

The stress tests were conducted for optimal water allocations in the node-and-link system. The 14 sub-basins are forced by atmospheric drivers (i.e., precipitation and temperature) to generate natural streamflow. The generated streamflows are regulated to meet the water demands and instreamflow requirements. The operations should be constrained by geomorphological and management conditions. We used a conceptual runoff model and an optimization model for evaluating water supply and ecological performances with stochastic weather series perturbed by hypothetical climate stresses.

3.3.1 Generating climate-stress-induced weather series

The stochastic weather generator (WG) by Steinschneider and Brown (2013) was employed to produce plausible daily precipitation and temperature sequences with climatic perturbations (i.e., generating climate stresses). Several bottom-up assessments successfully used this model to evaluate performance of hydrologic systems under varying climate stresses (e.g., Whateley et al., 2014; Steinschneider et al., 2015b).

Two stochastic models are combined in the semi-parametric WG. The wavelet autoregressive model proposed by Kwon et al. (2007) first generates annual precipitation series spatially-averaged within a region of interest for a desired length (20 years in this study). The wavelet components of the annual precipitation series are extended by the autoregressive model to embed the low-frequency structure inherent in observations. Then, daily weather series conditioned by the random annual precipitation are simulated by the Markovian bootstrap resampler of Apipattanavis et al. (2007). In this process, the daily observations are resampled by the k-nearest-neighbour scheme and the precipitation occurrence series generated by the standard Markovian process (e.g., Wilks, 1998). The weather data at multiple locations within the region of interest are sampled together for spatial coherence. As the final step, the mean and variance of stochastic precipitation series are adjusted by the ordinary QM to impose climatic perturbations stresses. The temperature series are simply perturbed by adding a temperature differential. Further in-depth details about the stochastic WG are found in Steinschneider and Brown (2013).

To examine the water supply performance under climatic stresses, we generated 539 sets of precipitation and temperature time series spatially coherent between the 14 sub-basins. The perturbations imposed on the precipitation time series were changes in the mean of non-zero daily precipitation and its coefficient of variance (CV). The applied mean changes of precipitation were from -60% to +40% at 10% increments relative to the observations for 1973-2015, while the CV changes

were from -40% to +80% at 20% increments (i.e., 11×7 perturbations for precipitation). The temperature time series were perturbed by adding 0-6 ℃ at 1℃ increments (i.e., 7 perturbations for temperature). Thus, the total number of the climatic perturbations was 11×7×7=539. The 539 sets of climate-stress-induced weather series were input to a rainfall-runoff model to quantify natural water flows at the sub-basins. To develop the logistic response surfaces, each weather series generated by the WG were summarized by three bi-decadal properties of the mean annual precipitation (P_{avg}), the CV of daily precipitation (P_{cv}), and the mean annual temperature (T_{avg}).

3.3.2 Simulating natural runoff at the sub-basin nodes

A simple rainfall-runoff model, GR4J (Perrin et al., 2003), was used to simulate natural flows at the sub-basins nodes. GR4J has been frequently employed in many studies under diverse climates, such as parameter regionalization (e.g., Oudin et al., 2010), predicting flow durations (e.g., Zhang et al., 2015), and low flow estimations (e.g. Demirel et al., 2015) among many others. GR4J uses four conceptual parameters to describe functional behaviours of a watershed in response to lumped precipitation and potential evapotranspiration (PET) inputs. The parameters implicitly explain soil water storage, groundwater exchange, routing storage, and excess runoff generations within a watershed. The parsimonious structure of GR4J poses relatively small equifinality problem in parameter calibration and regionalization (Oudin et al., 2008; Perrin et al., 2010). Perrin et al. (2003) provides the computation procedures in detail.

In the case study, a proximity-based regionalization was applied for parameter identification, because almost no natural streamflow observations are available at the outlets of the sub-basins. The operational inflow records at the Yongdam Dam were the only applicable observations for parameter calibration at the sub-basin 3001. For the other sub-basins, the parameter sets were transferred from neighbouring watersheds assessed in Kim et al. (2017). Kim et al. (2017) comparatively assessed performance of the proximity-based parameter transfer in comparison to several alternative methods, concluding that spatial proximity well captured functional similarity between 45 gauged watersheds in South Korea. The mean Nash-Sutcliffe efficiency (NSE) was 0.53 with a standard deviation of 0.41, when transferring the parameter sets of five neighbouring catchments calibrated with observed hydrographs (Kim et al., 2017). Hence, for the 13 sub-basins from 3002 to 3014, natural flows were simulated with the transferred parameter sets from five nearby gauged watersheds, while flows at the sub-basin 3001 were generated by the parameters calibrated against the inflow data. The five runoff simulations were averaged for the sub-basins in which the regionalization scheme was used. The parameter set calibrated against the inflow records for the sub-basin 3001 yielded a NSE value of 0.62 for 2007-2015. The daily natural flows simulated by GR4J with the 539 stochastic weather sets were temporally aggregated at monthly values for water allocation modelling.

3.3.3 Water allocation modelling

The total water availability in the river basin during a certain month is water storages in the dams and reservoirs at the end of the previous month plus the natural flows at the sub-basins in the current month. Some of the available water is again kept in the storage facilities for supplying water in upcoming months. Thus, operators' decisions on water storages in each month

recursively affect supply performance in the river basin through a bi-decadal period. A monthly sequential optimization model was used to determine amounts of the water storages and consumptions at each sub-basin. The operators should to minimize water deficiency during a current month, while the water storages need to be maximized for water supplies in upcoming months. We assumed that the two conflicting objectives are equally important for the operators. Hence, the objective function to determine water supplies and storages at the nodes for a particular month was:

$$\text{Minimize } \frac{\sum D_i - \sum S_i}{\sum D_i} - \frac{\sum V_i - \sum C_i}{\sum C_i} \quad (2a)$$

$$D_i = DA_i + DM_i \quad (2b)$$

$$S_i = SA_i + SM_i \quad (2c)$$

where, D_i is the total demand, S_i is the total supply, V_i is the water storage, and C_i is the storage capacity (C_i) at node i. SA_i and SM_i are agricultural and M&I water supplied for agricultural (DA_i) and M&I demands (DM_i) at node i, respectively. The total water demand at each node (D_i) is the sum of agricultural demand (DA_i) and M&I demand (DM_i). Likewise, the water supply at each node is divided into agricultural supply (SA_i) and M&I supply (SM_i).

The monthly optimizations were subject to constraints. The water supply (S_i) to a demand node was limited by water availability, which is the sum of natural flow at the node in the current month, flows from other nodes via the stream and the human-made links in the current month, and water storage at the node in the previous month. Water surplus at the nodes was not allowed (i.e., $S_i \leq D_i$). The water remained after supplies and storage at a sub-basin node should be discharged from the node through the channel network. The water storage at each node is constrained by its storage capacity ($V_i \leq C_i$). The water transfers through the human-made links were only supplied for M&I demands of destination nodes, and were limited by the conveyance capacity (40 $Mm^3\,month^{-1}$). The agricultural and M&I demands were of equal priorities in optimizations.

With 20-year-long natural flows per climatic perturbation, we determined SA_i, SM_i, and V_i month by month using the global optimization tool "fmincon" in the Matlab software. Since V_i values determined for a month become water availability for its next month, optimizations for 240 months interplay sequentially. To consider the return flows, we followed the assumptions in the water plan for 2020 (MOLIT, 2016). Simply, 65% of the M&I water use at each node was assumed to return and become available water for following nodes, while no return flows after agricultural uses were considered in the water plan due to high water use efficiency.

3.3.4 Evaluating water supply and ecological performances

Using the optimized SA_i, SM_i, and V_i values, water supply performances at the demand nodes were measured for the given 20-year-long stress-imposed weather series. For each sub-basin node, we measured the water supply reliability ($\rho_{s,i}$) defined as the probability of satisfactory supply against 99% of the monthly demands:

$$\rho_{s,i} = \text{prob}\,[S_i \geq 0.99 D_i] \quad (3)$$

The amount of water passing the seven locations with the instreamflow requirements can be also calculated using the decision variables and the natural flows. The environmental reliability at a instramflow location j ($\rho_{e,j}$) was evaluated by:

$$\rho_{e,j} = \text{prob}\left[F_j \geq F_{min,j}\right] \quad (4)$$

where, F_j and $F_{min,j}$ are the flow passing location j and the instream flows required for ecosystem sustainability at the location, respectively.

In total, water reliabilities at the 14 demand nodes (14 sub-basins) and the 7 locations requiring instreamflows were evaluated for each climatic perturbation. These 21 sets of performance indicators were used to develop the logistic response functions for each sub-basin node and instreamflow location with corresponding climate stress. To develop the logistic surfaces, we assumed that the stakeholder-driven thresholds for $\rho_{s,i}$ and $\rho_{e,j}$ were 0.95 and 0.70, respectively. The 539 sets of P_{avg}, P_{cv}, and T_{avg} that represent the perturbed weather series were categorized into zero and one against the two thresholds for the logistic regressions.

4 Results

4.1 Water supply performance at the sub-basins

The stress tests that forced the system models (i.e., GR4J and the optimization model) by the perturbed weather series produced 539 sets of reliabilities for each sub-basin and each location of instreamflow. Figure 2 displays the scatter plots between water supply reliability (ρ_s) at the sub-basin 3001 and corresponding changes in P_{avg}, P_{cv}, and T_{avg} relative to 1996-2015. We preliminarily checked statistical significance of the explanatory variables using the multiple linear regressions. The changes in P_{avg} and T_{avg} were of very high significance to variation of the ρ_s values (p-values < 10^{-16}), whereas the change in P_{cv} was insignificant (p-value = 0.744). This indicates that the bi-decadal water supply reliability is generally determined by variations of the mean precipitation and temperature for a bi-decadal period. Though higher precipitation variability (P_{cv}) could generate more direct runoff across the river basin, storage capacities of the agricultural reservoirs and dams seem to nullify the impacts of P_{cv} changes on the variation of water supply reliability. The preliminary regression analysis led us to a hypothesis that changes in P_{avg} and T_{avg} could sufficiently capture the variation of water supply reliabilities across the river basin.

Figure 3a illustrates the regression function between the ρ_s values and changes in P_{avg} and T_{avg} (R^2 = 0.93), on which the collection of 50 GCM projections was overlaid. Most of the 50 GCMs expected that ρ_s at the sub-basin 3001 would be greater than 0.95 for 2020-2039. This type of response surfaces between expected performance and hypothetical climatic

stresses have been commonly used in the decision-centric assessments (e.g., Brown et al., 2012; Whateley et al., 2014; Turner et al., 2014). Figure 3c indicate that ρ_s at the sub-basin 3001could be less than 0.95, if P_{avg} decreases by 30% approximately. The ρ_s values varied significantly even with zero decrease in P_{avg}, indicating that there might be the risk of unsatisfactory supply performance even with no changes in P_{avg}.

The risk of $\rho_s < 0.95$ could be evaluated by the logistic surface shown in Figure 3b. The sigmoid functions fitted to binary outcomes categorized against the threshold of $\rho_s > 0.95$ (Figure 3d) could provide approximate probabilities of $\rho_s > 0.95$ (hereafter referred to as π_{s95}) at the sub-basin 3001. π_{s95} declined with rising temperatures, since water availability was reduced by evaporation losses. The π_{s95} values indicated by the 50 GCMs ranged between 74 and 99% for 2020-2039. It should be noted that the climatic bound for $\rho_s = 0.95$ (dashed lines in Figure 3a and b) has the risk of $\rho_s < 0.95$ at 40-60% of chances on the logistic surfaces. It seems that there still exist considerable risks of unsatisfactory performances on the zone of satisfactory performance in Figure 3a.

Likewise, we fitted the sigmoid functions to the binary outcomes against the threshold of $\rho_s > 0.95$ for the other sub-basins. Figure 4 displays the climatic bounds at which $\pi_{s95} = 95\%$ for each sub-basin. The sub-basin 3001 was of the highest bound among the 14 sub-basins, indicating that the uppermost sub-basin is the most vulnerable to changes in P_{avg} and T_{avg}. 15 GCMs were located below the climate boundary of the sub-basin 3001. On the contrary, the boundary of the sub-basin 3012 was the lowest. For every GCM projections, π_{s95} at the sub-basin 3012 was larger than 99%. The sub-basins with limited connections to the upper sub-basins tend to have higher climatic bounds of $\pi_{s95} = 95\%$. The lower sub-basins receiving streamflow generated by the upper sub-basins were likely to withstand stronger climate stresses, even though they have relatively large agricultural demands.

4.2 Environmental reliability against the instreamflow requirements

We compared the modelled flows at the 7 locations of instreamflow against the minimum requirements, and evaluated the environmental reliabilities (i.e., ρ_e) at each location. Figure 5 shows the box plots of ρ_e values at the seven locations in response to the 539 climate perturbations. While ρ_e values at all the locations decreased as climate became drier, the location E was the most vulnerable. Even with no changes in P_{avg} and T_{avg}, the outflows from the sub-basin 3011 were often less than the minimum requirement, implying that ecosystems near the location E might be currently undermined by the large agricultural and M&I demands at the sub-basin 3011. If P_{avg} decreased by 20% and T_{avg} rose by 3℃, ρ_e at the location E would fall below 0.5. On the other hand, streamflow at the location D perfectly satisfied the instreamflow requirement under the same stress. Despite the second-largest M&I demands at the sub-basin 3009, water transfers from the two large dams could deliver sufficient water supplies. 65% of the water supplies for M&I demand was supposed to return to the stream network and became streamflow to meet the instreamflow requirement at the location D. Although both sub-basins 3009 and 3011 have limited geomorphological connectivity to the upper sub-basins, their demand components and linkages to the two large dams made the significant difference between their ρ_e values.

We developed the logistic response surfaces with binary outcomes against the threshold of $\rho_e > 0.70$ at which the instreamflow requirement at the location E were satisfied in the optimization model under no climate stresses (i.e., no changes in P_{avg} and T_{avg} relative to 1996-2015) Figure 6 displays the climatic bounds at which the probability of $\rho_e > 0.70$ (hereafter referred to as π_{e70}) is 95% for all the locations requiring instreamflow. As expected, the bound for the location E was the highest, and the climate zone for $\pi_{e70} > 95\%$ sensitively declines with rising T_{avg}. The bound for $\pi_{s95} = 95\%$ at the sub-basin 3001 (black dashed line) was below the bounds for the locations E. The human-demand-only operations would increase the risks of ecosystem degradation near the locations E if climate becomes drier. The environmental risks at the locations E seem to be more sensitive to rising T_{avg} than the water supply risk at the sub-basin 3001. Only 5 out of the 50 GCMs for 2020-2039 (10%) indicate $\pi_{e70} > 95\%$ at the location E.

4.3 Consideration of the instreamflow into water management

From the assessments with the logistic surfaces and the GCM projections, the environmental risk at the location E was likely to become an issue for 2020-2039. As an adaptation strategy, the instreamflow could be considered in water management to be balanced between water supply and environmental risks. We modelled this management option by including the instreamflow requirement at the location E in the objective function of the water allocation model as:

$$\text{Minimize } \frac{\sum D_i - \sum S_i}{\sum D_i} - \frac{\sum V_i - \sum C_i}{\sum C_i} + w\frac{Q_{min,E} - Q_E}{Q_{min,E}} \quad (4)$$

where, $Q_{min,E}$ and Q_E are the instreamflow requirement and flow at the location E, respectively. w is a weight representing relative importance of the instreamflow in water management. While the instreamflow requirement at the location E could be treated as a constraint for optimizations, this approach may lead to no optimal solutions under severe climate stresses. Hence, it would be better to consider the instreamflow requirement in the objective function for the stress tests.

Through trial and error experiments with the 539 climate perturbations, we found that ρ_e at the location E could considerably increase with a tiny w value. The sequential optimizations with w=0.01 allowed us to have a fairly improved ρ_e value at the location E. However, we found that the improved ecological reliability at the location E was by substantial reduction in water supply reliability at the sub-basin 3002. Figure 7 illustrates the logistic models for water supply at the sub-basin 3002 and the instreamflow requirement at the location E under the two operation options applied to the case study. The first operation was only considering the given agricultural and M&I demands (O_1), whereas the deficit against the instreamflow requirement was considered in the second option (O_2). By changing the operation objective from O_1 to O_2, the risk of $\rho_e < 0.95$ at the sub-basin substantially increased at the sub-basin 3002. The risk of unsatisfactory water supply was found even with increasing P_{avg} under O_2. Indeed, the water supply performance became much more sensitive to T_{avg} changes. Conversely, the risk of unsatisfactory ecological reliability at the location E substantially declined. This is because the optimization model did not increase discharge from the sub-basin 3011 for the instreamflow requirement due to the high

agricultural demands. Instead, the model forced to increase outflows from the Yongdam dam to meet the agricultural demands at the sub-basins 3012 and 3014 and the instreamflow at the location E. It was inevitable to have deficient water supplies in the sub-basin 3002 with relatively small demands even under optimized water allocations. In other words, minimizing total water deficiency of the entire basin may force the local water deficit in the sub-basin 3002.

4.4 Assessing the management options with the EEDC framework

The two operation options applied in the case study were assessed with the logistic surfaces for the all the sub-basins and the instreamflow locations simultaneously (Figure 8). Table A2 summarizes all the logistic regressions applied in the case study. We simply used the boundaries of π_{s95} = 95% and π_{e70} = 95% for the assessment. With the logistic surfaces, the system robustness to climate change could be measured in the same manner proposed in the original EEDC framework (Poff et al., 2016).

By comparing the middle panels in Figure 8, it is indicated that considering the instreamflow in the objective function significantly lowered the climatic bound of π_{e70} = 95% at the location E, thereby widening the climatic zone within which all the locations mutually satisfy π_{e70} > 95%. However, in trade-off, the bound of π_{s95} = 95% for the sub-basin 3002 moved upward, narrowing the climatic zone mutually satisfying π_{s95} > 95% for all the demand nodes. Overall, the climatic zone mutually satisfying π_{s95} > 95% and π_{e70} > 95% for all the sub-basins and instreamflow locations was expected to decrease when the instreamflow requirement at the location E was considered. Based on the reduced mutual climate zone, considering the instreamflow requirement in operations would slightly decrease overall system robustness to climate stresses.

In summary, water supply reliabilities at the sub-basins 3001 and 3002 would be the most vulnerable to climate stresses. The highest environmental risks from climate change would be found at the locations E in terms of the instreamflow requirements. To reduce the environmental risk at the location E, fairly increasing risks of $\rho_s \leq 0.95$ at the sub-basin 3002 should be accepted. Only 4 out of the 50 GCMs indicated $\pi_{s95} > 0.95$.

5 Discussion and conclusions

5.1 Use of the logistic surfaces for climat change impact assessment

The response surfaces allowed users to estimate expected performances of hydrologic systems in response to climate stressors, providing convenience to promptly evaluate many GCM projections (e.g., Turner et al., 2014; Brown et al., 2012; Prudhomme et al., 2010). Nevertheless, they could provide insufficient probabilistic information needed for decision-making processes. A possible approach to evaluating the risk of unsatisfactory performances was to count the GCM projections satisfying a pre-defined threshold (e.g.., Moursi et al., 2017; Brown et al., 2012). However, the GCM counts are highly dependent on the size of the GCM collections. Even in the case that all the GCMs in users' hand fall within the favourable climate zone on the response surfaces, it does not guarantee that future system performance will be satisfactory at 100% confidence.

The logistic response surface could supplement the weakness of the response surfaces. It enables to directly evaluate the risk of system failures from a single climate projection. The probability estimates from the logistic surfaces can play a role in risk-based decision-making particularly when an adaptive solution is targeted at a particular climate prediction (e.g., resizing infrastructures for a reference climate condition). The logistic surface developed for the adaptive solution may directly provide the risk of system failures under the climate prediction.

One concern in the logistic surfaces may be validity of the probability estimates, since the sigmoid function is hypothetical. Hence, we attempted to comparatively evaluate the π_{s95} and π_{e70} values from the logistic surfaces using a typical stochastic resampling with the same system models. For the validation, three arbitrary perturbations were selected as (-37.1%, +2.5℃), (-27.7%, +1.3℃), (-13.6%, +0.6℃) for P_{avg} and T_{avg}, respectively. Then, 100 sets of 20-year-long weather series were generated for each perturbation using the stochastic weather generator, and the system models were forced by the generated weather series. By counting the cases satisfying $\rho_s > 0.95$ or $\rho_e > 0.70$ among the 100 simulations, the probability estimates at the sub-basins and instreamflow locations were obtained for each perturbation. Figure 9 shows the 1:1 plot comparing the probability estimates gained from the stochastic sampling and the logistic regressions for the three perturbations. The probability estimates from the two approaches agreed approximately. The stochastic sampling was to quantify the impacts of internal climate variability within a bi-decadal period; however, it may require unacceptable computational costs. 300 sets of stress tests were necessary only for the three perturbations. The 1:1 plot in Figure 9 may imply that the impacts of internal climate variability could be approximately captured by the logistic regression that described collective behaviours of the 539 stress tests. If affordable, a more rigorous validation may be possible with a higher number of stochastic weather generations with additional perturbations.

5.2 Eco-engineering decision scaling with the logistic surfaces

The EEDC framework (Poff et al., 2016) integrates the responsive behaviours of multiple performance metrics into a single climate space. By measuring the size of the climate zone mutually satisfying the multiple criteria, decision-makers can perceive the robustness of system performance with conflicting interests. The decision-makers may select solutions that can widen the mutual climate zone for robust adaptations to climate change. Poff et al. (2016) provided a prominent example that assessed adaptation costs and potential environmental risks with this framework in order to find the most robust strategies in a dam site to climate change. In this study, we showed the advantage of this framework to explore performances at many sub-components of a large system in a single climate domain.

One difference between this study and Poff et al. (2016) is that we used the logistic climate bounds to measure the size of the mutual climate zone satisfying the multiple probabilistic thresholds. Since the original EEDC framework was focused on expected performances, a question can be raised as to "what if no climate projections fall within the mutual climate zone?" In this case, stakeholders may perceive unacceptable risks even though an adaptive solution can enlarge the mutual climate zone for multiple criteria. By its nature, the EEDC considering multiple criteria should have a narrower acceptable climate zone than single-criterion assessments. If the logistic response surfaces were employed instead, users can simultaneously

measure how much system robustness can be obtained from an adaptive solution and how much risks of unsatisfactory performances are indicated by climate projections. They may be necessary information for decision-making processes.

5.3 Limitations

There are several caveats in the case study. First, the monthly operations to balance between water scarcity and storages might be only a part of operators' interests. The stakeholders in practice may have conflicting interests (e.g., reducing flood risks vs. increasing water storage) rather than taking actions toward the single objective. Thus, this study should be deemed a special case focused on the maximum supply reliability under the given operational objectives. A validated simulation model for water allocation will be needed for a more realistic application.

Second, it was unavoidable for us to use many simplifications and assumptions for modelling optimal water managements in the study river basin with complicated features (e.g., monthly dam operations and simple temperature perturbations). Given the substantial uncertainty sources associated with system models, the risks of system failures might be greater than our assessments. The logistic surfaces in this work would only consider the impacts of internal climatic variability on system performances.

5.4 Conclusions

In this study, we proposed to incorporate the logistic regression into a decision-centric framework for probabilistic impact assessments. The proposed approach requires no more stress tests than typical response-surface-based assessments, albeit some validation is needed. Thus, it may be an efficient method to support risk-based decision making processes. Following conclusions are worth emphasizing:

(1) The logistic surfaces can provide convenience to explore potential risks of system failures when a pre-defined threshold is available, while the response surface can show system performance. On the logistic surfaces, the risk of system failures could be directly indicated by individual GCMs.

(2) Within the eco-engineering decision scaling framework, the logistic surfaces can be flexibly used to evaluate robustness of hydrological systems to climate stressors. Multi-faceted stakeholders' interests can be considered in a domain of probability.

(3) The case study for the Geum River Basin in South Korea provides an assessment that the human-demand-only operations would make the eco-systems increasingly vulnerable. To consider the instreamflow requirement in operations for 2020-2039, risks of insufficient water supply should increase at the upper sub-basins with small water demands.

Acknowledgement

This study was supported by the APEC Climate Center. We send special thanks for the water demand data provided by the team leading for the national water resources plan at the Korea Institute of Civil Engineering and Building Technology. The

GCMs downscaled by Dr. Hyung-Il Eum at the Alberta Environment and Parks are greatly appreciated. All authors declare no conflict of interests. The data required to reproduce the results are available upon request from the authors (d.kim@apcc21.org, sjchoi@kict.re.kr).

References

Apipattanavis, S., Podesta, G., Rajagopalan, B., and Katz, R. W.: A semiparametric multivariate and multisite weather generator, Water Resour. Res., 43, W11401, https://doi.org/10.1029/2006WR005714., 2007

Bae, D.-H., Jung, I.-W., and Chang, H: Long-term trend of precipitation and runoff in Korean river basins, Hydrol. Process., 22, 2644–2656, 2008.

Brown, C. M., Lund, J. R., Cai, X., Reed, P. M., Zagona, E. A., Ostfeld, A., Hall, J., Characklis, G. W., Yu, W., and Brekke, L.: The future of water resources systems analysis: Toward a scientific framework for sustainable water management, Water Resour. Res., 51, 6110–6124, https://doi.org/10.1002/2015WR017114, 2015.

Brown, C., and Wilby, R. L.: An alternate approach to assessing climate risks. Eos Trans. AGU, 93(41), 401, 2012.

Brown, C., Ghile, Y., Laverty, M., and Li, K.: Decision scaling: linking bottom-up vulnerability analysis with climate projections in the water sector. Water Resour. Res., W09537, https://doi.org/10.1029/2011WR011212, 2012.

Bürger, G., Sobie, S. R., Cannon, A. J., Werner, A. T., and Murdock, T. Q.: Downscaling extremes: an intercomparison of multiple methods for future climate. J. Clim., 26(10), 3429–3449, https://doi.org/10.1175/JCLI-D-12-00249.1, 2013.

Cannon, A. J., Sobie, S. R., and Murdock, T. Q.: Bias correction of GCM precipitation by quantile mapping: How well do methods preserve changes in quantiles and extremes?, J. Clim. 28, 6938-6959, 2015.

Cosgrove, W. J., and Loucks, D. P.: Water management: Current and future challenges and research directions, Water Resour. Res., 51, 4823–4839, https://doi.org/10.1002/2014WR016869, 2015.

Culley, S., Noble, S., Yates, A., Timbs, M., Westra, S., Maier, H. R., Giuliani, M., and Castelletti, A.: A bottom-up approach to identifying the maximum operational adaptive capacity of water resource systems to a changing climate, Water Resour. Res., 52, 6751–6768, https://doi.org/10.1002/2015WR018253, 2016.

Daly, C., Halbleib, M., Smith, J. I., Gibson, W. P., Doggett, M. K., Taylor, G. H., Curtis, J., and Pasteris, P. P.: Physiographically sensitive mapping of climatological temperature and precipitation across the conterminous United States, Int. J. Climatol., 28, 2031-2064, https://doi.org/10.1002/joc.1688, 2008.

Demirel, M. C., Booij, M. J., and Hoekstra, A. Y.: The skill of seasonal ensemble low-flow forecasts in the Moselle River for three different hydrological models, Hydrol. Earth Syst. Sci., 19, 275-291, https://doi.org/10.5194/hess-19-275-2015, 2015.

Deser, C., Phillips, A., Bourdette, V., and Teng, H.: Uncertainty in climate change projections: the role of internal variability, Clim. Dyn., 38, 527-546, doi:10.1007/s00382-010-0977-x., 2012.

Dufresne, J.-L., and Bony, S.: An assessment of the primary sources of spread of global warming estimates from coupled atmosphere-ocean models, J. Clim., 21, 5135-5144, 2008.

Eum, H.-I., and Cannon, A. J.: Intercomparison of projected changes in climate extremes for South Korea: Application of trend preserving statistical downscaling methods to the CMIP5 ensemble. Int. J. Climatol., 37(8), 3381-3397, 2017.

Eum, H.-I., and Simonovic, S. P.: Integrated reservoir management system for adaptation to climate change: The Nakdong River Basin in Korea, Water Resour. Manage., 24, 3397-3417, 2010.

Georgakakos, A. P., Yao, H., Kistenmacher, M., Georgakakos, K. P., Graham, N. E., Cheng, F.-Y., Spencer, C., and Shamir, E.: Value of adaptive water resources management in Northern California under climatic variability and change: Reservoir management, J. Hydrol., 412-413, 34-46, https://doi.org/ 10.1016/j.jhydrol.2011.04.038, 2012.

Haasnoot, M., Kwakkel, J. H., Walker, W. E., and ter Maat, J.: Dynamic adaptive policy pathways: A method for crafting robust decisions for a deeply uncertain world, Glob. Environ. Change, 23, 485-498, 2013.

Hadka, D., Herman, J., Reed, P., and Keller, K.: An open source framework for many-objective robust decision making, Environ. Model. Softw., 74, 114-129, 2015.

Hwang, S. and Graham, W. D.: Development and comparative evaluation of a stochastic analog method to downscale daily GCM precipitation, Hydrol. Earth Syst. Sci., 17, 4481-4502, https://doi.org/10.5194/hess-17-4481-2013, 2013.

Jowett, I. G.: Instream flow methods: a comparison of approaches. Regul. Rivers: Res. Mgmt., 13, 115-127, 1997.

Jung, Y., and Eum, H.-I.: Application of a statistical interpolation method to correct extreme values in high-resolution gridded climate variables, J. Clim. Chang. Res., 6, 331-334, 2015.

Kay, A. L., Crooks, S. M., and Reynard, N. S.: Using response surfaces to estimate impacts of climate change on flood peaks: assessment of uncertainty, Hydrol. Process., 28, 5273–5287, https://doi.org/ 10.1002/hyp.10000, 2014.

Kim,.D., Chun, J. A., and Aikins, C. M.: An hourly-scale scenario-neutral flood risk assessment in a mesoscale catchment under climate change, Hydrol. Process., 32, 3416–3430, https://doi.org/10.1002/hyp.13273, 2018.

Kim, D., Jung, I. W., and Chun, J. A.: A comparative assessment of rainfall–runoff modelling against regional flow duration curves for ungauged catchments, Hydrol. Earth Syst. Sci., 21, 5647-5661, https://doi.org/10.5194/hess-21-5647-2017, 2017.

Korean Meteorological Administration (KMA) Climatological normals of Korea (1981–2010). Publ. 11-1360000-000077-14, Korea Meteorological Administration, 678 pp. [Available online at http://www.kma.go.kr/down/Climatological_2010.pdf.], 2011.

Korteling, B., Dessai, S., and Kapelan, Z.: Using information-gap decision theory for water resources planning under Severe Uncertainty, Water Resour. Manage., 27, 1149-117, https://doi.org/10.1007/s11269-012-0164-4, 2013.

Kwon, H.-H., Lall, U., and Khalil, A. F.: Stochastic simulation model for nonstationary time series using an autoregressive wavelet decomposition: Applications to rainfall and temperature, Water Resour. Res., 43, W05407, https://doi.org/10.1029/2006WR005258, 2007.

Lampert, R. J., and Groves, D. G.: Identifying and evaluating robust adaptive policy responses to climate change for water management agencies in the American west, Technol. Forecasting Soc. Change, 77, 960-974, 2010.

Ministry of Construction and Transportation (MOCT): National Water Resources Plan (Water Vision 2020), Daejeon, South Korea, 2000.

Ministry of Construction and Transportation (MOCT): National Water Resources Plan (2006-2020), Daejeon, South Korea, 2006.

Ministry of Land, Transport and Maritime Affairs (MLTM): National Water Resources Plan (2011-2020), Daejeon, South Korea, 2011.

Ministry of Land, Infrastructure and Transport (MOLIT): National Water Resources Plan (2001-2020) – 3rd revision (2016-2020), 2016.

Moursi, H., Kim, D., and Kaluarachchi, J. J.: A probabilistic assessment of agricultural waer scarcity in a semi-arid and snowmelt-dominated river basin under climate change, Agric. Water Manage., 193, 142-152, 2017.

Oudin, L., Kay, A., Andréassian, V., and Perrin, C.: Are seemingly physically similar catchments truly hydrologically similar?, Water Resour. Res., 46, W11558, https://doi.org/10.1029/2009WR008887., 2010.

Oudin, L., Andréassian, V., Perrin, C., Michel, C., and Le Moine, N.: Spatial proximity, physical similarity, regression and ungaged catchments: a comparison between of regionalization approaches based on 913 French catchments, Water Resour. Res., 44, W03413, https://doi.org/10.1029/2007WR006240, 2008.

Perrin, C., Michel, C., and Andréassian, V.: Improvement of a parsimonious model for streamflow simulation, J. Hydrol., 279, 275-289, 2003.

Perrin, C., Oudin, L., Andreassian, V., Rojas-Serna, C., Michel, C., and Mathevet, T.: Impact of limited streamflow data on the efficiency and the parameters of rainfall-runoff models, Hydrolog. Sci. J., 52, 131-151, https://doi.org/10.1623/hysj.52.1.131, 2010.

Poff, N. L., Brown, C. M., Grantham, T. E., Matthews, J. H., Palmer, M. A., Spence, C. M., Wilby, R. L., Haasnoot, M., Mendoza, G. F., Dominique, K. C., and Baeza, A.: Sustainable water management under future uncertainty with eco-engineering decision making, Nature Clim. Change, 6, 25-34. https://doi.org/10.1038/nclimate2765, 2016.

Prudhomme, C., Wilby, R. L., Crooks, S., Kay, A. L., and Reynard, N. S.: Scenario-neutral approach to climate change impact studies: Application to flood risk, J. Hydrol., 390, 198-209. https://doi.org/10.1016/j.jhydrol.2010.06.043., 2010.

Rosenberg, D. E.: Blended near-optimal alternative generation, visualization, and interaction for water resources decision making, Water Resour. Res., 51, 2047–2063, https://doi.org/10.1002/2013WR014667., 2015.

Schlef, K. E., Steinschneider, S., and Brown, C. M.: Spatiotemporal impacts of climate and demand on water supply in the Apalachicola-Chattahoochee-Flint Basin, J. Water Resour. Plann. Manage., 144, 05017020, 2017.

Stainforth, D. A., Aina, T., Christensen, C., Collins, M., Faull, N., Frame, D. J., Kettleborough, J. A., Knight, S., Martin, A., Murphy, J. M., Piani, C., Sexton, D., Smith, L. A., Spicer, R. A., Thorpe, A. J., and Allen, M.R.: Uncertainty in predictions of the climate response to rising levels of greenhouse gases, Nature, 433, 403-406, 2005.

Steinschneider, S., and Brown, C: A semiparametric multivariate, multisite weather generator with low-frequency variability for use in climate risk assessments, Water Resour. Res., 49, 7205–7220. https://doi.org/10.1002/wrcr.20528, 2013.

Steinschneider, S., and Brown, C.: Dynamic reservoir management with real-option risk hedging as a robust adaptation to nonstationary climate, Water Resour. Res. 48, W11525. https://doi.org/10.1029/2011WR011318, 2012.

Steinschneider, S., McCrary, R., Wi, S., Mulligan, K., Mearns, L. O., and Brown, C.: Expanded decision-scaling framework to select robust long-term water-system plans under hydroclimatic uncertainties, J. Water Resour. Plann. Manage., 141, 04015023-1, 2015a.

Steinschneider, S., Wi, S., and Brown, C.: The integrated effects of climate and hydrologic uncertainty on future flood risk assessments, Hydrol. Process., 29, 2823–2839. https://doi.org/10.1002/hyp.10409, 2015b.

Stevens, B. and Bony, S.: What are climate models missing?, Science, 340, 1053-1054, 2013.

Turner, S. W. D., Marlow, D., Ekström, M., Rhodes, B. G., Kularathna, U., and Jeffrey, P. J.: Linking climate projections to performance: A yield-based decision scaling assessment of a large urban water resources system, Water Resour. Res., 50, 3553–3567, https://doi.org/10.1002/2013WR015156, 2014.

Weaver, C. P., Lempert, R. J., Brown, C., Hall, J. A., Revell, D., and Sarewitz, D.: Improving the contribution of climate model information to decision making: the value and demands of robust decision frameworks, WIREs Clim. Change, 4: 39–60. https://doi.org/10.1002/wcc.202, 2013.

Whateley, S., and Brown, C.: Assessing the relative effects of emissions, climate means, and variability on large water supply systems, Geophys. Res. Lett., 43, 11329–11338, https://doi.org/10.1002/2016GL070241, 2016

Whateley, S., Steinschneider, S., and Brown, C.: A climate change range-based method for estimating robustness for water resources supply, Water Resour. Res. 50, 8944-8961, https://doi.org/10.1002/WR015956, 2014.

Whateley, S., Steinschneider, S., and Brown, C.: Selecting stochastic climate realizations to efficiently explore a wide range of climate risk to water resource systems, J. Water Resour. Plann. Manage., 142, 06016002, 2016.

Wilby, R. L. and Dessai, S.: Robust adaptation to climate change, Weather, 65: 180-185, https://doi.org/10.1002/wea.543, 2010.

Wilks, D.: Multisite generalization of a daily stochastic precipitation generation model, J. Hydrol., 210, 178-191, 1998.

Woodward, M. , Kapelan, Z. and Gouldby, B.: Adaptive flood risk management under climate change uncertainty using real options and optimization, Risk Analysis, 34, 75-92, https://doi.org/10.1111/risa.12088, 2014.

Xu, W., Zhao, J., Zhao, T., and Wang, Z: Adaptive reservoir operation model incorporating nonstationary inflow prediction, J. Water Resour. Plann. Manage., 141, 04014099, 2015.

Yan, D., Werners, S. E., Ludwig, F., and Huang, H.Q.: Hydrological response to climate change: the Pearl River, China under different RCP scenarios, J. Hydrol. Reg. Stud., 4, 228–245, 2015.

Zhang, Y., Vaze, J., Chiew, F. H. S., and Li, M.: Comparing flow duration curve and rainfall-runoff modelling for predicting daily runoff in ungauged catchments, J. Hydrol., 525, 72-86, 2015

Zhang, Y., You, Q., Chen, C., and Ge, J.: Impacts of climate change on streamflows under RCP scenarios. A case study in Xin River Basin, China, Atmos. Res. 178, 521–534, 2016.

Appendix 1. List of the General Circulation Models and summary of the logistic regressions.

Table A1. List of the selected GCMs for the impact assessment under the RCP 4.5 and 8.5 scenarios.

No.	Model Name	Resolution (degree)	Producing Institution
1	CMCC-CM	0.750×0.748	Centro Euro-Mediterraneo per I Cambiamenti Climatici
2	CCSM4	1.250×0.942	National Center for Atmospheric Research
3	CESM1-BGC	1.250×0.942	
4	CESM1-CAM5	1.250×0.942	
5	MRI-CGCM3	1.125×1.122	Meteorological Research Institute
6	CNRM-CM5	1.406×1.401	Centre National de Recherches Meteorologiques
7	HadGEM2-AO	1.875×1.250	Met Office Hadley Centre
8	HadGEM2-CC	1.875×1.250	
9	HadGEM2-ES	1.875×1.250	
10	INM-CM4	2.000×1.500	Institute for Numerical Mathematics
11	IPSL-CM5A-MR	2.500×1.268	Institut Pierre-Simon Laplace
12	MPI-ESM-LR	1.875×1.865	Max Planck Institute for Meteorology (MPI-M)
13	MPI-ESM-MR	1.875×1.865	
14	FGOALS-s2	2.813×1.659	LASG, Institute of Atmospheric Physics, Chinese Academy of Sciences
15	NorESM1-M	2.500×1.895	Norwegian Climate Centre
16	GFDL-ESM2G	2.500×2.023	Geophysical Fluid Dynamics Laboratory
17	GFDL-ESM2M	2.500×2.023	
18	BCC-CSM1-1	2.813×2.791	Beijing Climate Center, China Meteorological Administration
19	BCC-CSM1-1-M	1.125×1.122	
20	IPSL-CM5A-LR	3.750×1.895	Institut Pierre-Simon Laplace
21	IPSL-CM5B-LR	3.750×1.895	
22	MIROC5	1.406×1.401	Atmosphere and Ocean Research Institute, National Institute for Environmental Studies, and Japan Agency for Marine-Earth Science and Technology
23	MIROC-ESM-CHEM	2.813×2.791	
24	MIROC-ESM	2.813×2.791	
25	CanESM2	2.813×2.791	Canadian Centre for Climate Modelling and Analysis

Table A2. The summary of the logistic regressions. The explanatory variables were statistically significant (p-values < 10^{-3}) for the all regression models. R^2 is the McFadden pseudo R^2.

		O_1: Human-demand-only operation				O_2: Considering the instreamflow at E			
		Regression coefficients			R^2	Regression coefficients			R^2
		Intersect	ΔP_{avg} (%)	ΔT_{avg} (℃)		Intersect	ΔP_{avg} (%)	ΔT_{avg} (℃)	
Sub-basin	3001	4.38	0.245	-0.630	0.825	3.55	0.234	-0.529	0.813
	3002	14.5	0.401	-0.900	0.878	1.86	0.189	-0.883	0.752
	3003	12.8	0.368	-0.776	0.869	10.3	0.312	-0.605	0.850
	3004	14.1	0.388	-0.872	0.873	13.2	0.363	-0.760	0.865
	3005	12.3	0.405	-0.724	0.887	12.9	0.426	-0.806	0.892
	3006	16.8	0.430	-0.922	0.879	13.6	0.354	-0.812	0.858
	3007	8.97	0.338	-0.866	0.874	7.42	0.295	-0.812	0.858
	3008	21.0	0.528	-1.03	0.898	18.2	0.465	-0.954	0.887
	3009	10.3	0.302	-0.527	0.842	10.3	0.302	-0.527	0.842
	3010	23.6	0.507	-0.654	0.894	22.5	0.470	-0.761	0.883
	3011	11.2	0.383	-0.736	0.882	11.9	0.410	-0.765	0.889
	3012	24.0	0.493	-0.825	0.885	22.5	0.458	-0.790	0.875
	3013	11.4	0.292	-0.396	0.826	11.0	0.284	-0.384	0.821
	3014	21.2	0.439	-0.690	0.871	21.9	0.448	-0.729	0.872
Instreamflow locations	A	28.1	0.644	-1.69	0.920	27.6	0.634	-1.67	0.919
	B	11.1	0.432	-1.11	0.904	10.7	0.423	-1.00	0.902
	C	6.43	0.370	-1.25	0.882	6.51	0.399	-1.31	0.889
	D	25.9	0.445	-0.638	0.800	21.1	0.402	-0.49	0.827
	E	1.47	0.282	-1.08	0.823	7.02	0.533	-1.51	0.912
	F	5.44	0.332	-1.12	0.868	6.52	0.385	-1.32	0.886
	G	14.1	0.591	-1.58	0.934	13.0	0.547	-1.38	0.929

Table 1: Annual agricultural and M&I demands per demand node and the minimum instream flows from the sub-basins corresponding to the seven locations.

	ID No.	Mean annual flow* ($Mm^3\ yr^{-1}$)	Agricultural demand ($Mm^3\ yr^{-1}$)	M&I demand ($Mm^3\ yr^{-1}$)	Total storage capacity (Mm^3)	Instream flow requirement ($Mm^3\ month^{-1}$)
Sub-basin node	3001	639.6	50.9	7.6	29.7	
	3002	97.3	4.0	0.4	1.0	
	3003	254.5	13.1	2.4	5.0	
	3004	498.6	50.5	15.8	10.1	8.9 (A)
	3005	382.8	42.3	5.1	14.9	6.6 (B)
	3006	82.6	9.2	3.3	6.8	
	3007	384.0	74.2	6.1	22.0	7.4 (C)
	3008	473.6	36.9	34.4	7.2	
	3009	465.8	31.5	208.5	7.0	6.7 (D)
	3010	92.2	19.3	16.4	0.2	20.8 (E)
	3011	1145.0	356.6	296.2	100.9	
	3012	1437.2	367.9	75.1	38.4	45.9 (F)
	3013	506.1	193.2	26.4	47.4	6.4 (G)
	3014	340.7	215.1	10.3	29.6	
Outside demand node	OD 1			20.6		
	OD 2			42.1		
	OD 3			5.1		
	OD 4			4.0		
Total		6,800.0	1464.7	779.8	320.2	

* Natural runoff averaged over 20-year rainfall-runoff simulations with stochastic weather series containing zero climatic perturbations ($\Delta P_{avg} = 0\%$, $\Delta P_{cv} = 0\%$, $\Delta T_{avg} = 0\%$) relative to 1996-2015.

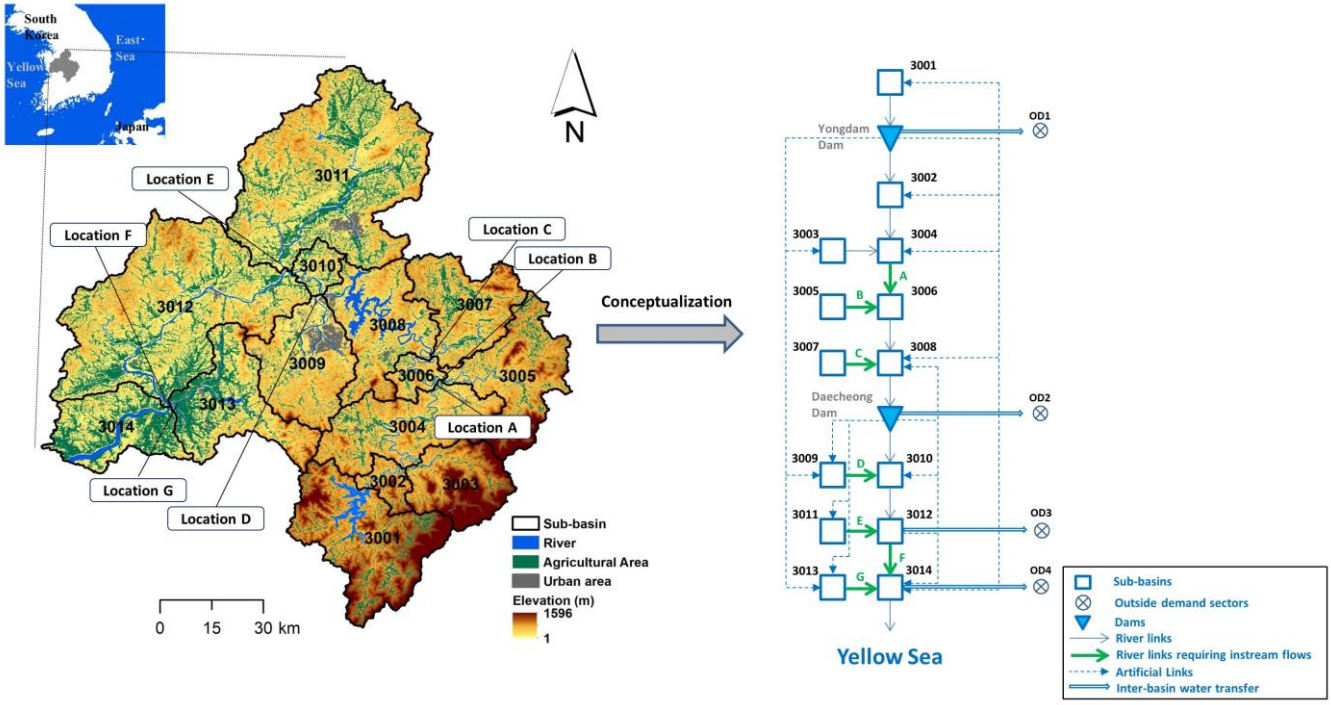

Figure 1: Layout of the Geum River Basins (left) and the simplified node-and-link network for modelling water allocations (right).

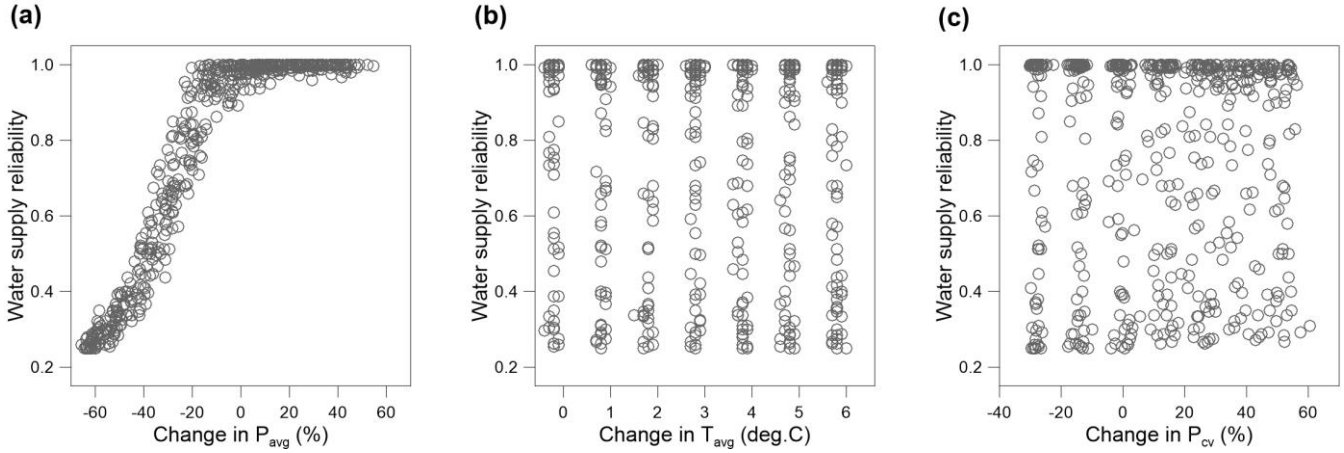

Figure 2: Scatter plots between the water supply reliability at the sub-basin 3001 and changes in (a) P_{avg}, (b) T_{avg}, and (c) P_{cv} collected from the stress tests driven by the 539 sets of stochastically generated stress-imposed weather series.

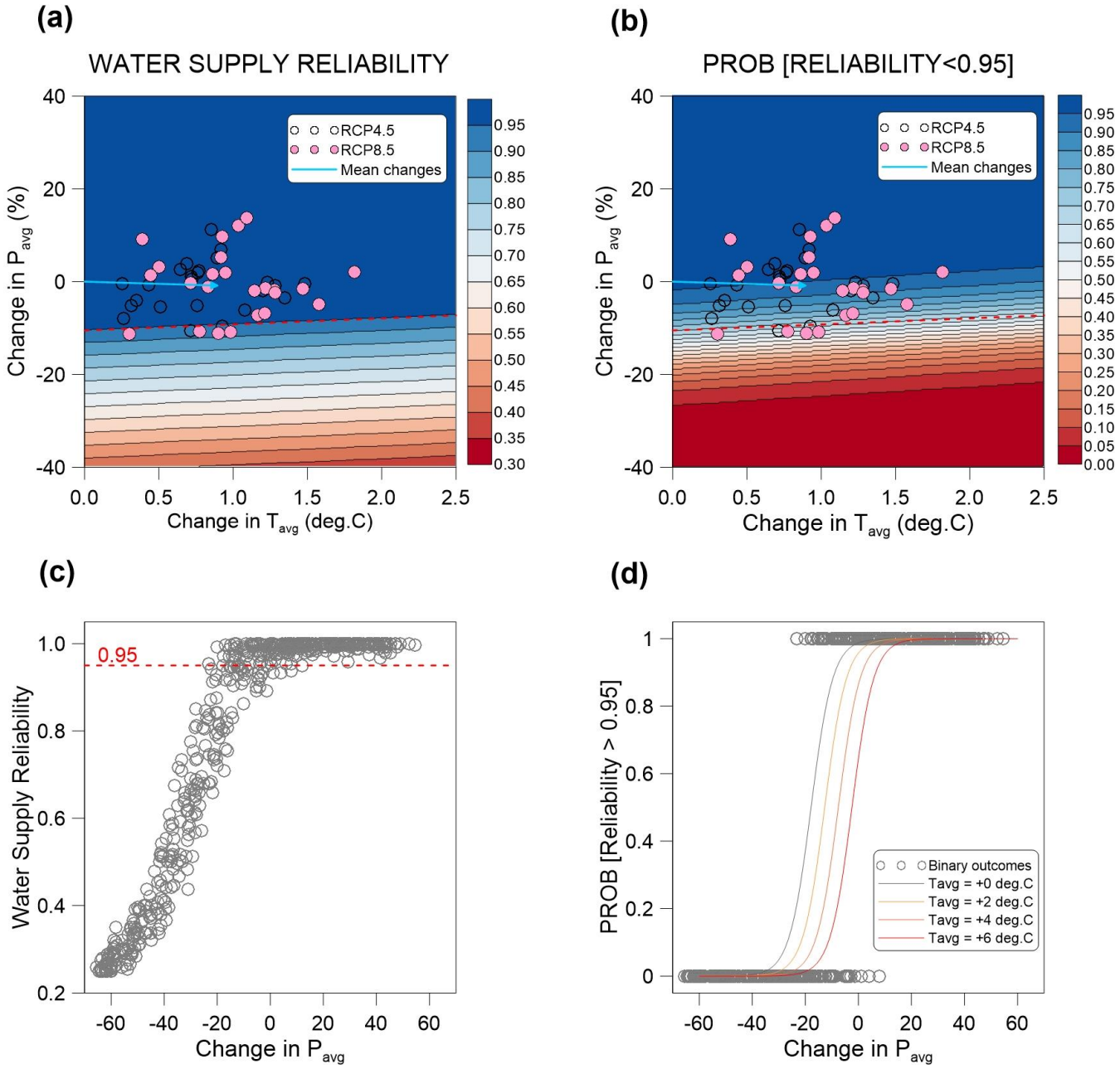

Figure 3: (a) Response surface of ρ_s at the sub-basin 3011, (b) logistic response surface of the probability of $\rho_s > 0.95$. (c) the scatter plot between ρ_s and change in P_{avg}, (d) the binary outcomes against the threshold of $\rho_s > 0.95$ and the sigmoid functions for the probability of $\rho_s > 0.95$. The empty and filled circles overlaid on (a) and (b) are the 50 GCM projections for 2020-2039. The dashed lines in (a) and (b) are the climatic bounds for the climatic threshold of ρ_s=0.95.

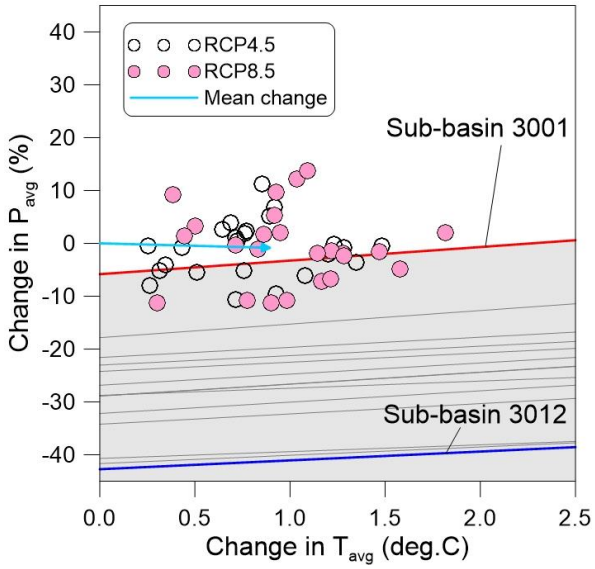

Figure 4: Climatic bounds for Prob[ρ_s>0.95]=95% for the 14 sub-basins, on which the 50 GCM projections for 2020-2039 were superimposed.

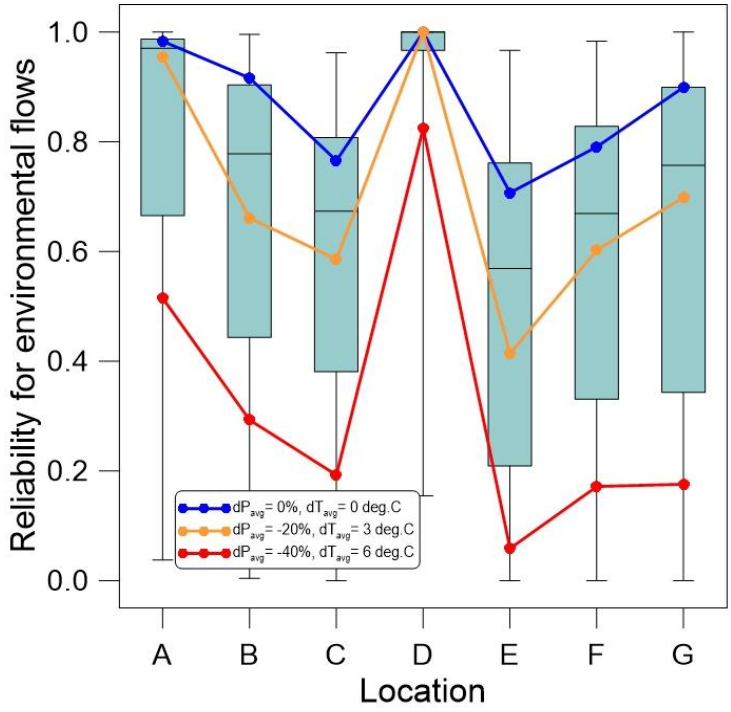

Figure 5: Reliability against the instream flow requirements at the seven locations obtained from the 539 sequential optimizations with stress-induced weather series. The blue, grey, and red lines connect the reliabilities at the seven locations under the three representative climatic stresses.

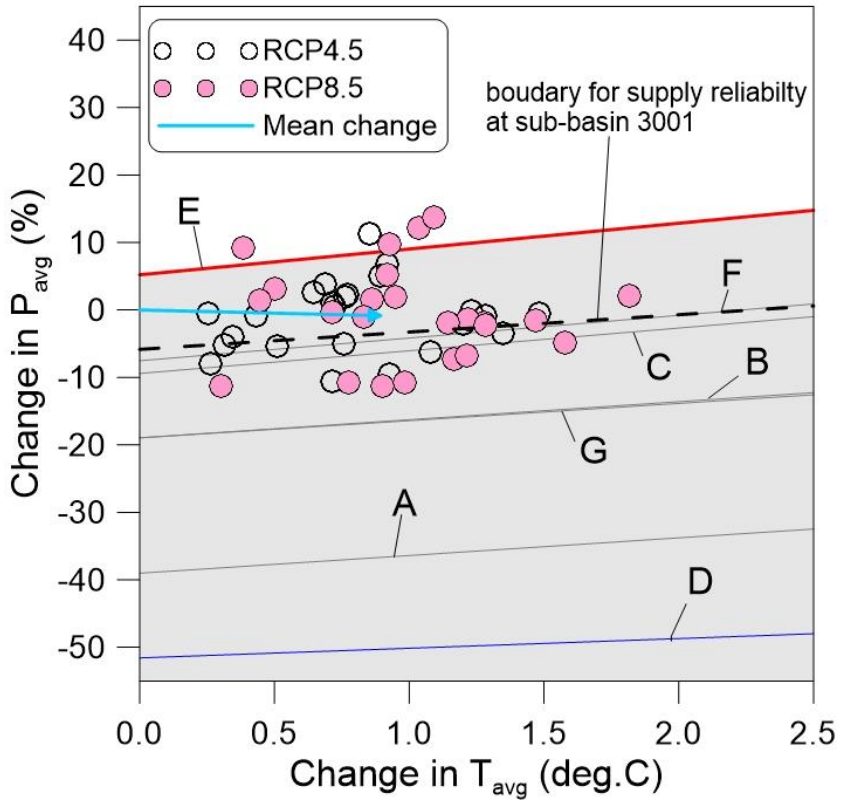

Figure 6: As in Figure 4, but for the probability of ρ_e>0.70 at the seven locations of instreamflow.

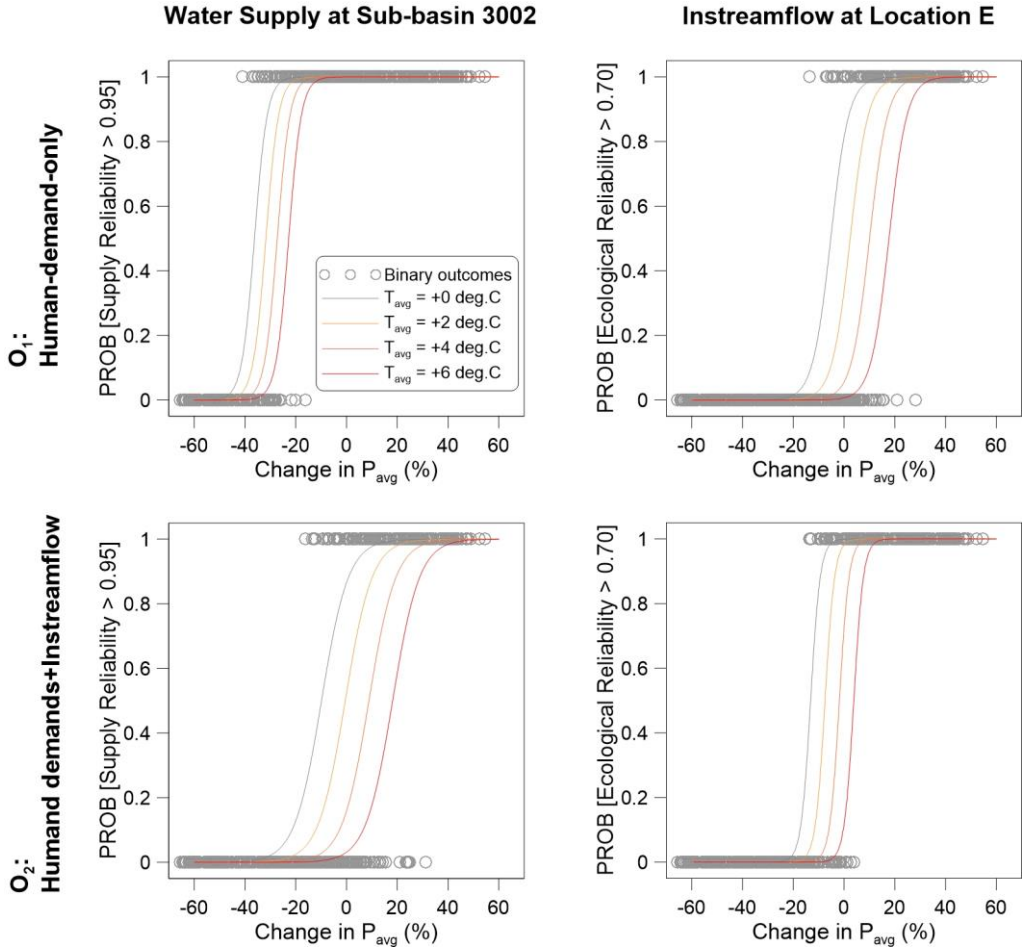

Figure 7: The logistic regression models for π_{s95} at the sub-basin 3002 (left) and π_{e70} at the location E (right) under the human-demand-only operation (upper) and the operation considering human demands and instreamflow together (lower)

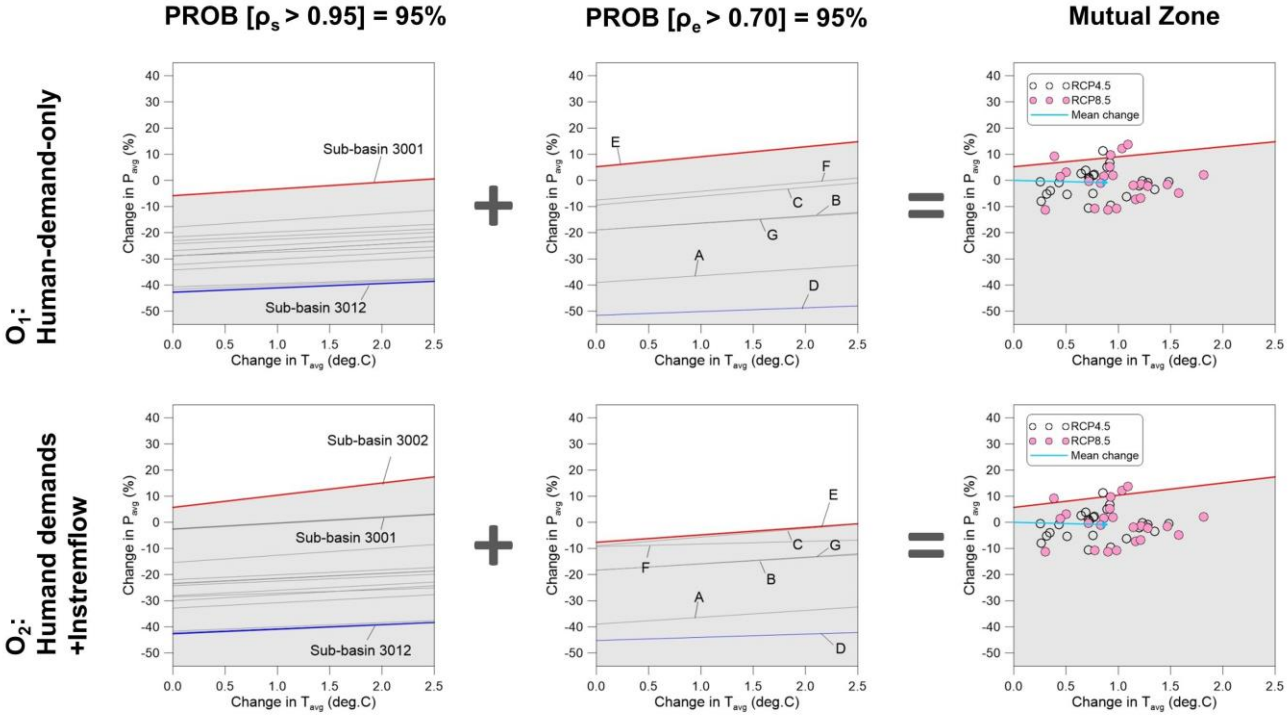

Figure 8: Climatic bounds for π_{s95} = 95% (left) and π_{e70} = 95% (middle), and the bound mutually satisfying both criteria (right) under the human-demand-only operations (top) in comparison to the operations considering the instream flows at the location E (bottom). The empty and filled circles are the 50 GCM projections for 2020-2039.

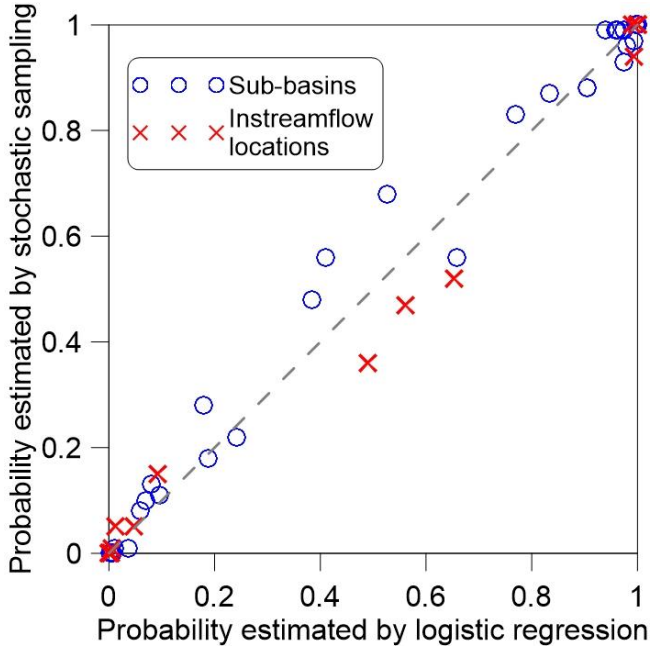

Figure 9: 1:1 plots between the probabily estimates from the stochastic sampling and those from the logistic regressions for the case study.